

**PFLOTRAN: Massively Parallel 3D Simulator for  
CO<sub>2</sub> Sequestration in Geologic Media**

Chuan Lu and Peter C. Lichtner  
Los Alamos National Laboratory  
Los Alamos, New Mexico

## Abstract

Geologic sequestration in depleted oil reservoirs, saline aquifers, etc. has been proposed as an effective way to stabilize the concentration of CO<sub>2</sub> in the atmosphere and thus mitigate its effect on global climate change. We have developed a massively parallel 3-D reservoir simulator PFLOTRAN for modeling supercritical CO<sub>2</sub> sequestration in geologic formations based on continuum scale mass and energy conservation equations. The simulator incorporates the effects of CO<sub>2</sub> and H<sub>2</sub>O dissolution and diffusion in the aqueous and CO<sub>2</sub>-rich phases, respectively. The mass and energy equations are sequentially coupled to reactive transport equations describing multi-component chemical reactions within the formation including aqueous speciation and precipitation and dissolution of minerals, including CO<sub>2</sub>-bearing phases, to describe aqueous and mineral CO<sub>2</sub> sequestration. The effect of injected CO<sub>2</sub> on pH, CO<sub>2</sub> concentration within the aqueous phase, mineral stability, and other factors can be evaluated with this model. The multiphase flow field is coupled to changes in porosity and permeability of the geologic porous medium caused by precipitation and dissolution reactions of minerals. Parallelization is carried out using the PETSc parallel library package based on MPI providing high parallel efficiency and allowing simulations with several tens of millions of degrees of freedom to be carried out—ideal for large-scale field applications involving multi-component chemistry. A lookup table provides rapid evaluation of the H<sub>2</sub>O and CO<sub>2</sub> equations of state. Several examples are presented which examine the predicted distribution and fate of CO<sub>2</sub> injected into a subsurface geologic system and evaluate the numerical efficiency of the simulator.

## 1 Introduction

Recently researchers at the Mauna Loa volcano laboratory at the Climate Monitoring Diagnostics Laboratory directed by NOAA (National Oceanic and Atmospheric Administration) have recorded a record increase in CO<sub>2</sub> to 378 ppm (March 31, 2005). To mitigate the continuous increase in the atmospheric concentration of CO<sub>2</sub>, geologic disposal of CO<sub>2</sub> has been suggested as an attractive alternative. Three storage mechanisms can be identified for subsurface geologic sequestration of CO<sub>2</sub>: (*i*) as a separate gas phase or supercritical fluid (phase trapping); (*ii*) dissolved in groundwater (solubility trapping); and (*iii*) precipitated as secondary minerals such as calcite, magnesite, dawsonite, etc. (mineral trapping). To investigate the effectiveness of these different sequestration mechanisms, numerical modeling is essential for gaining an understanding of the fate of CO<sub>2</sub> injected in subsurface geologic formations over time spans of tens of thousands of years. However, one must be cautious that model simulations reflect reality and are not contaminated by numerical effects and lack of adequate understanding of the fundamental processes involved. For example, density differences in the CO<sub>2</sub> enriched brine have been shown to cause instabilities leading to convective mixing and more rapid dissolution of supercritical CO<sub>2</sub> into the brine compared to diffusion alone (Ennis-King and Paterson, 2003; Garcia, 2003). To capture these processes requires high grid resolution to resolve fingering patterns or, alternatively, development of new upscaling techniques that would allow these processes to be adequately described at larger grid scales. In this contribution the parallel computer model PFLOTRAN is introduced and applied to an example of sequestration of CO<sub>2</sub> in a sandstone formation.

The computational effort necessary to carry out such an investigation for a realistic 3D field site is enormous. Length scales involved range from the size of the geologic formation itself, on the order of kilometers, to much smaller length scales characteristic of fingering phenomena on the order of meters or less to chemical interactions that may be smaller than centimeters. For example, to discretize a domain 1 km × 1 km × 500 m with  $100 \times 100 \times 100 = 10^6$  nodes leads to a typical grid block size of 10 m × 10 m × 5 m, or roughly the size of a small conference room. For a grid block of this size, features that require smaller scales for their resolution such as fingering, and chemical interactions may be lost. Not accounting for these processes may give erroneous predictions for the rate of sequestration of the CO<sub>2</sub> plume over time. Incorporating chemical processes may require anywhere from 5–15 additional degrees of freedom per node, depending on the sophistication of the simulation and what processes are deemed important. This will depend on the type of host rock (limestone, granite, sandstone, etc.), and the time scale of the simulation. The longer the simulation time the more important become slowly reacting minerals such as feldspars and

clay minerals.

Obtaining solutions to these large systems of equations calls for a massively parallel implementation to reduce both computation time and memory requirements. For example, assuming ideal speedup running a problem with ten million nodes on 500 processors is roughly equivalent to running a problem with 20,000 nodes on a single processor workstation—a relatively small sized problem. With present day computational facilities, a single processor may have 4GB or more of RAM, which is more than adequate to solve millions of equations using fully implicit Newton-Krylov techniques employing domain decomposition. This approach is described in more detail in what follows for the computer code PFLOTRAN. This code solves equations for multiphase-multicomponent reactive flow and transport for nonisothermal, variably saturated porous media for implementation either on a single workstation or massively parallel computing architectures.

It is important to note that supercomputing alone cannot solve the problem of fine-scale resolution needed to describe local chemical environments and other processes. In a three dimensional problem, reducing the grid spacing in each direction by a factor of two requires eight times as many processors to keep the load on each processor the same. In order to capture smaller scale effects an approach is required that allows information at the sub-grid scale to be incorporated into the model, such as a dual continuum model, requiring additional computational resources.

## **2 PFLOTRAN: Massively Parallel, Multiphase-Multicomponent Flow & Transport Model**

The computer code PFLOTRAN solves a coupled system of mass and energy conservation equations for the two-phase system consisting of supercritical CO<sub>2</sub> and H<sub>2</sub>O. PFLOTRAN describes coupled thermal-hydrologic-chemical (THC) processes in variably saturated, nonisothermal, porous media in one (1D), two (2D), or three (3D) spatial dimensions. PFLOTRAN may be used to describe systems involving two-phase fluid flow consisting of liquid water and CO<sub>2</sub> (or air), and multicomponent reactive chemical transport involving aqueous, gaseous and mineral species. The model is currently being extended to include three phases H<sub>2</sub>O-CO<sub>2</sub>-gas.

The code PFLOTRAN consists of two distinct modules: a mass and energy flow code (PFLOW), and a reactive transport code (PTRAN). The module PFLOW solves mass conservation equations for water and CO<sub>2</sub> and an energy balance equation. For supercritical CO<sub>2</sub>, the Span and Wagner (1996) equation of state for pure CO<sub>2</sub> is used. The module PTRAN solves mass conservation equations for a multicomponent geochemical system. Chemical reactions included in the module PTRAN consist of homogeneous aqueous speciation reactions, heterogeneous gaseous speciation and mineral precipitation and dissolution reactions, and ion-exchange and sorption reactions. The rates of mineral reactions are described through kinetic rate laws. The rates of homogeneous aqueous reactions may be described using either a kinetic description or by imposing local equilibrium. Both PFLOW and PTRAN are based on a fully implicit solution of the governing equations.

The modules PFLOW and PTRAN may be run either in standalone or coupled mode. In coupled mode the flow velocities of liquid and supercritical CO<sub>2</sub> phases, saturation, pressure, and temperature computed from the module PFLOW are fed to the transport module PTRAN. Both transient and steady-state coupled modes are possible. In the transient mode, the modules PFLOW and PTRAN are sequentially coupled allowing for changes in porosity and permeability due to chemical reactions to alter the flow field. In steady-state mode, the module PFLOW is called first until a steady state is established, and then the module PTRAN is called which uses the steady-state flow field computed from PFLOW as input. Both modules apply generally to heterogeneous porous media.

Chemical reactions included in PTRAN involve aqueous species and minerals which can be written in

the general form

$$\sum_j \nu_{ji} \mathcal{A}_j \rightleftharpoons \mathcal{A}_i, \quad (1)$$

and

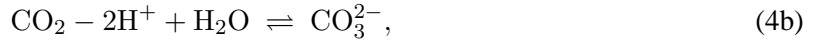
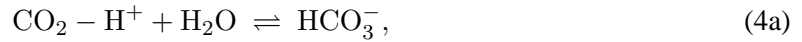
$$\sum_j \nu_{jm} \mathcal{A}_j \rightleftharpoons \mathcal{M}_m, \quad (2)$$

respectively, where the set of species  $\{\mathcal{A}_j\}$  refer to a set of primary or basis species in terms of which all other species are written,  $\mathcal{A}_i$  denotes an aqueous complex referred to as a secondary species, and  $\mathcal{M}_m$  refers to a mineral. The corresponding thermodynamic equilibrium constants  $K_i$ ,  $K_m$ , and reaction stoichiometric coefficients  $\nu_{ji}$ ,  $\nu_{jm}$  are derived from an extensive database for aqueous species, gases, and minerals. Partitioning  $\text{CO}_2$  between  $\text{H}_2\text{O}$  and supercritical  $\text{CO}_2$  is accomplished with the reaction



where the subscript (g) refers to the supercritical phase and (aq) to the aqueous phase. Other reactions not include above that may also significantly impact  $\text{CO}_2$  sequestration are ion exchange and surface complexation reactions.

Examples of Eqs.(1) and (2) for an aqueous fluid reacting with calcite consist of the following reaction network



described by the 4 primary species:  $\text{Ca}^{2+}$ ,  $\text{H}^+$ ,  $\text{H}_2\text{O}$ , and  $\text{CO}_2$ . The first four reactions involve only aqueous species and are referred to as homogeneous reactions. These reactions are considered to be sufficiently fast that local chemical equilibrium applies. The remaining reaction involves the solid phase calcite and thus is referred to as a heterogeneous reaction. The rate of mineral reactions is governed by kinetics and requires knowledge of the mineral surface area and kinetic rate constant for the reaction. The predominance field of each secondary species changes in proximity to the supercritical  $\text{CO}_2$  plume with the fluid becoming more acidic in the neighborhood of the plume. Generally, the aqueous fluid is in a state of partial equilibrium with respect to the solid phase.

## 2.1 Mass and Energy Conservation Equations: PFLOW & PTRAN

PFLOTTRAN solves a coupled system of mass and energy conservation equations for the two-phase system consisting of supercritical  $\text{CO}_2$  and  $\text{H}_2\text{O}$ . The code consists of two sequentially coupled routines PFLOW and PTRAN, which may also be run separately in standalone mode. Briefly the equations solved by PFLOW for mass and energy conservation can be summarized as:

$$\frac{\partial}{\partial t} \phi s_l \rho_l X_w^l + \nabla \cdot [\mathbf{q}_l \rho_l X_w^l - \phi s_l D_l \rho_l \nabla X_w^l] = -R_w + Q_w^l, \quad (5a)$$

$$\frac{\partial}{\partial t} \phi s_g \rho_g X_w^g + \nabla \cdot [\mathbf{q}_g \rho_g X_w^g - \phi s_g D_g \rho_g \nabla X_w^g] = R_w + Q_w^g, \quad (5b)$$

$$\frac{\partial}{\partial t} \left[ \phi (s_l \rho_l X_c^l + s_g \rho_g X_c^g) \right] + \nabla \cdot \left[ \mathbf{q}_l \rho_l X_c^l + \mathbf{q}_g \rho_g X_c^g - \phi (s_l D_l \rho_l \nabla X_c^l + s_g D_g \rho_g \nabla X_c^g) \right] = Q_c, \quad (5c)$$

$$\frac{\partial}{\partial t} \left[ \phi (s_l \rho_l U_l + s_g \rho_g U_g) + (1 - \phi) \rho_r c_r T \right] + \nabla \cdot (\mathbf{q}_l \rho_l H_l + \mathbf{q}_g \rho_g H_g - \kappa \nabla T) = Q_e. \quad (5d)$$

In these equations, phases  $l$  and  $g$  refer to liquid water and supercritical CO<sub>2</sub>, respectively, species are designated by  $w = \text{H}_2\text{O}$ ,  $c = \text{CO}_2$ ,  $\phi$  denotes porosity of the geologic formation,  $s_l = 1 - s_g$  refer to liquid and gas saturation;  $X_i^\pi$ , ( $\pi = l, g$ ), denotes the mole fraction of species  $i = \text{CO}_2, \text{H}_2\text{O}$ ;  $\rho_\pi$ ,  $H_\pi$ ,  $U_\pi$  refer to the molar density, enthalpy, and internal energy of each fluid phase, respectively;  $\mathbf{q}_\pi$  denotes the Darcy flow rate defined by

$$\mathbf{q}_\pi = -\frac{k k_\pi}{\mu_\pi} \nabla (p_\pi - W_\pi \rho_\pi g z), \quad (6)$$

where  $k$  refers to the water saturated permeability,  $k_\pi$  denotes the relative permeability,  $\mu_\pi$  denotes the fluid viscosity,  $W_\pi$  denotes the formula weight, and  $g$  denotes the acceleration of gravity. The rate term  $R_w$  allows for a kinetic transition of H<sub>2</sub>O between liquid water and supercritical CO<sub>2</sub>. The source/sink terms  $Q_w$ ,  $Q_c$  and  $Q_e$ , describe injection and extraction at wells and provide coupling terms to the multi-species transport equations resulting from reaction with solids. This latter aspect is discussed in more detail below.

The flow equations may be rearranged in the equivalent, but more convenient form

$$\frac{\partial}{\partial t} [\phi (s_l \rho_l + s_g \rho_g)] + \nabla \cdot [\mathbf{q}_l \rho_l + \mathbf{q}_g \rho_g] = Q_w + Q_c, \quad (7a)$$

$$\frac{\partial}{\partial t} \phi s_l \rho_l X_w^l + \nabla \cdot [\mathbf{q}_l \rho_l X_w^l - \phi s_l D_l \rho_l \nabla X_w^l] = -R_w + Q_w^l, \quad (7b)$$

$$\frac{\partial}{\partial t} [\phi (s_l \rho_l X_w^l + s_g \rho_g X_w^g)] + \nabla \cdot [\mathbf{q}_l \rho_l X_w^l + \mathbf{q}_g \rho_g X_w^g - \phi (s_l D_l \rho_l \nabla X_w^l + s_g D_g \rho_g \nabla X_w^g)] = Q_w^l + Q_w^g, \quad (7c)$$

with the same energy conservation equation as above. This is the form of the flow equations actually solved by PFLOTTRAN.

In the approach used here the set of independent variables is fixed to four variables using  $p_{l,g}$ ,  $T$ ,  $s_{l,g}$ , and  $X_{\text{CO}_2}^{l,g}$ . The more commonly used variable switching approach (Pruess et al., 1999), requires specification of independent variables (3 in this case) at each node depending on the phases present to generate the residual and Jacobian.

The multicomponent reactive transport equations solved by PTRAN have the form

$$\frac{\partial}{\partial t} \left[ \phi (s_l \Psi_j^l + s_g \Psi_j^g) \right] + \nabla \cdot (\mathbf{\Omega}_j^l + \mathbf{\Omega}_j^g) = -\sum_m \nu_{jm} I_m, \quad (8)$$

for the  $j$ th primary species, and

$$\frac{\partial \phi_m}{\partial t} = \bar{V}_m I_m, \quad (9)$$

for the  $m$ th mineral, where  $\Psi_j^{l,g}$ ,  $\mathbf{\Omega}_j^{l,g}$  denote the total concentration and flux, defined by the expressions ( $\pi = l, g$ ),

$$\Psi_j^\pi = \delta_{\pi l} C_j^\pi + \sum_i \nu_{ji} C_i^\pi, \quad (10)$$

and

$$\mathbf{\Omega}_j^\pi = (-\tau \phi s_\pi D_\pi \nabla + \mathbf{q}_\pi) \Psi_j^\pi, \quad (11)$$

where  $C_j^\pi$  denotes the solute concentration in phase  $\pi$ ,  $C_i^\pi$  denotes the concentration of the  $i$ th secondary species related to the concentration of primary species through the mass action equations

$$C_i^\pi = (\gamma_i^\pi)^{-1} K_i^\pi \prod_j (\gamma_j^\pi C_j^\pi)^{\nu_{ji}^\pi}, \quad (12)$$

where  $\gamma_j^\pi$  denotes the activity coefficient,  $K_i^\pi$  the equilibrium constant for reaction (1). The mineral concentration is represented by the volume fraction  $\phi_m$  with molar volume  $\bar{V}_m$ . The kinetic reaction rate  $I_m$  for the  $m$ th mineral is assumed to have the form

$$I_m = -k_m A_m \Phi(\phi_m) (1 - K_m Q_m), \quad (13)$$

based on transition state theory, where  $k_m$  denotes the kinetic rate constant,  $K_m$  the equilibrium constant for reaction (2),  $A_m$  the mineral specific surface area, and  $Q_m$  the ion activity product defined by

$$Q_m = \prod_j (\gamma_j^\pi C_j^\pi)^{\nu_{jm}^\pi}. \quad (14)$$

The factor  $\Phi(\phi_m)$  is unity if  $\phi_m > 0$  or  $K_m Q_m > 1$ , and zero otherwise, where  $\phi_m$  denotes the mineral volume fraction. The sign of the rate is positive for precipitation and negative for dissolution and vanishes at equilibrium when  $K_m Q_m = 1$ .

## 2.2 Auxiliary Relations

The mass conservation equations must be augmented by various auxiliary relations given by

$$s_l + s_g = 1, \quad (15)$$

$$X_{\text{H}_2\text{O}}^\pi + X_{\text{CO}_2}^\pi = 1, \quad (\pi = l, g), \quad (16)$$

and

$$p_l = p_g - p_c, \quad (17)$$

where  $p_c$  denotes the capillary pressure given in terms of saturation by the following constitutive relation

$$p_c = \frac{1}{\alpha \beta_c} \left[ (s_l^e)^{1/m} - 1 \right]^{1-m}, \quad (18)$$

where the effective saturation is defined as

$$s_l^e = \frac{s_l - s_l^r}{1 - s_l^r}, \quad (19)$$

the quantity  $\beta_c \simeq 2$  gives the surface tension ratio between  $\text{CO}_2$ - $\text{H}_2\text{O}$  and air- $\text{H}_2\text{O}$ ,  $s_l^r$  denotes the residual saturation, and  $\alpha$  and  $m$  are van Genuchten parameters. Relative permeabilities for liquid water  $\text{H}_2\text{O}$  and supercritical  $\text{CO}_2$  are based on the formulation of Parker et al. (1987) for a multiphase system with the forms

$$k_{\text{H}_2\text{O}}^r = \sqrt{s_l^e} \left[ 1 - \left( 1 - (s_l^e)^{1/m} \right)^m \right]^2, \quad (20a)$$

$$k_{\text{CO}_2}^r = \sqrt{1 - s_l^e} \left[ 1 - \left( 1 - (1 - s_l^e)^{1/m} \right)^m \right]^7, \quad (20b)$$

Parameter values are derived from Holt et al. (1995) and Lindeberg and Holt (1994) determined from EOR by  $\text{CO}_2$  injection.

Henry's law is used to give the dissolved CO<sub>2</sub> concentration in H<sub>2</sub>O according to

$$x_{\text{CO}_2}^l = p_g \phi_{\text{CO}_2} K_{\text{CO}_2}^{-1}, \quad (21)$$

where  $\phi_{\text{CO}_2}$  denotes the fugacity coefficient. Henry's constant  $K_{\text{CO}_2}$  is based on the fit function from Crovetto (1991) modified for use with the Duan et al., (1992) EOS for pure CO<sub>2</sub> (Lichtner et al., 2003). This function has the form

$$\log K_{\text{CO}_2} = c_0 + \frac{1}{T} \left[ c_1 + c_3 \left( 1 - \frac{T}{T_{\text{H}_2\text{O}}^c} \right)^{1/3} \right] + \frac{c_2}{T^2}, \quad (22)$$

where  $T_{\text{H}_2\text{O}}^c$  denotes the critical temperature of pure H<sub>2</sub>O. A partial molar volume for CO<sub>2</sub> of  $\bar{V}_{\text{CO}_2} = 35$  cm<sup>3</sup>/mol was used to obtain the fit. Comparison of the calculated and experimental solubility of CO<sub>2</sub> in water as a function of temperature and pressure is shown in Figure (1). Data is taken from Dodds et al. (1956), Todheide and Franck (1963), and Takenouchi and Kennedy (1964). An approximate form of the mixture density for CO<sub>2</sub> dissolved in H<sub>2</sub>O is taken from Ennis-King and Paterson (2003) of the form

$$\rho_f = \rho_{\text{H}_2\text{O}} (1 + \alpha C_{\text{CO}_2}), \quad (23)$$

where  $\rho_f$  denotes the fluid density of the mixture,  $\rho_w$  is the density of pure water,  $C_{\text{CO}_2}$  denotes the concentration of CO<sub>2</sub>, and  $\alpha$  is a constant.

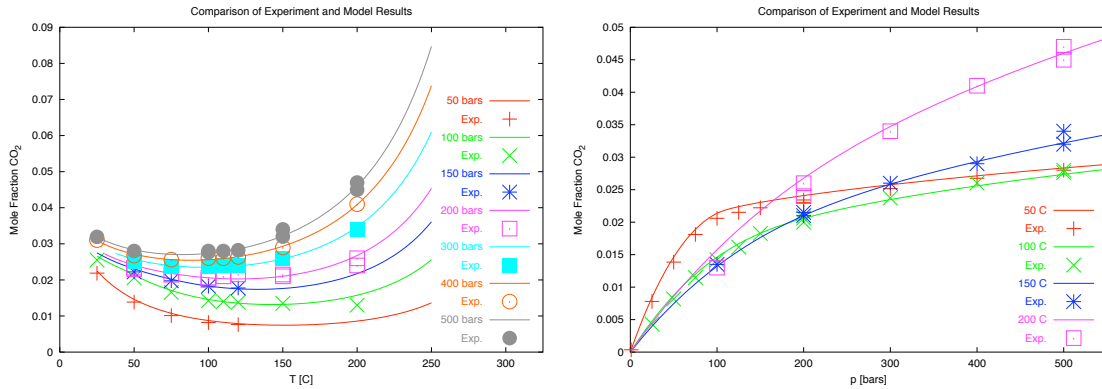


Figure 1: Comparison of the mole fraction of CO<sub>2</sub> in liquid water using a modified form of the Crovetto (1991) fit equation with experimental data as a function of temperature and pressure (Lichtner et al., 2003).

### 2.3 Coupling PFLOW and PTRAN

The routines PFLOW and PTRAN are solved sequentially. An option to iterate between the PFLOW and PTRAN solutions until a fully consistent solution is obtained will be implemented in the future. Generally PTRAN requires smaller time steps than PFLOW and therefore it is necessary to interpolate field variables passed from PFLOW to PTRAN at the desired time. A linear interpolation relation is used to obtain pressure, temperature, saturation, and Darcy velocities of the fluid phases at intermediate times between two PFLOW time steps  $t_1, t_2$ , using a relation of the form

$$\mathcal{F}(t) = \frac{t - t_1}{t_2 - t_1} \mathcal{F}_2 + \frac{t_2 - t}{t_2 - t_1} \mathcal{F}_1, \quad (24)$$

for  $t_1 \leq t \leq t_2$ , for field variable  $\mathcal{F}$ .

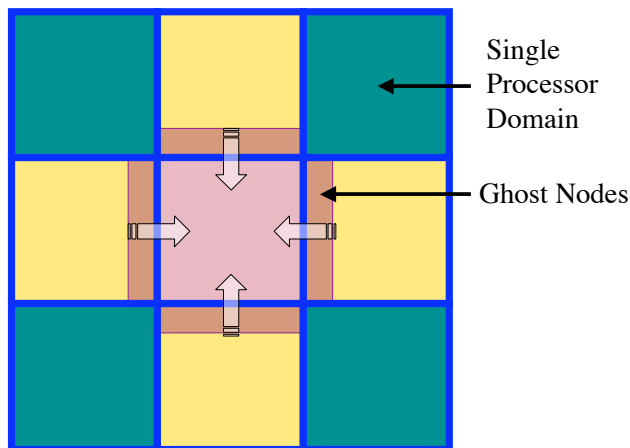


Figure 2: Schematic of domain decomposition showing position of ghost nodes and message passing indicated by arrows.

To account for changes in porosity and permeability due to mineral reactions, PTRAN is used to calculate an updated porosity over a time step  $\Delta t$  from the relation

$$\phi(\mathbf{r}, t + \Delta t) = \phi(\mathbf{r}, t) - \Delta t \sum_m \bar{V}_m I_m(\mathbf{r}, t + \Delta t), \quad (25)$$

and the revised porosity is passed back to PFLOW. Permeability is derived from porosity through a power law or other phenomenological relation.

In addition to porosity, it is also necessary to keep track of the amount of  $\text{H}_2\text{O}$  and  $\text{CO}_2$  consumed or produced by reactions with minerals and pass this rate from PTRAN back to PFLOW. In this regard there is redundancy in PFLOW and PTRAN, since both contain conservation equations for  $\text{CO}_2$  and  $\text{H}_2\text{O}$ . Dissolution of  $\text{CO}_2$  from the supercritical phase into liquid water is assumed to be governed by a local equilibrium relation based on Henry's constant and is therefore contained in the saturation variable.

### 3 Parallel Implementation

PFLOTRAN is written from the ground up to run on massively parallel computer architectures. Parallelization is implemented through the PETSc parallel library developed at Argonne National Laboratory (Belay et al., 1997). PETSc provides a user friendly set of routines for solving systems of nonlinear equations in parallel using domain decomposition. This includes parallel solvers and preconditioners, parallel construction of the Jacobian matrix and residual function, and seamless message passing, which together provide a high parallel efficiency. PETSc (latest version 2.3.0) has achieved a high level of maturity that allows rapid development with efficient parallel implementation for solving systems of non-linear partial differential equations. PFLOTRAN makes use of object-oriented features in FORTRAN 90 and is essentially platform independent, running on any machine that PETSc runs on. This includes laptop computers, workstations, and massively parallel high performance computing facilities.

A domain decomposition approach is used to provide a fully implicit solution to the governing equations based on iterative Newton-Krylov methods [see Figure (2)]. In this approach each processor is assigned a subdomain of the system and a parallel solve is implemented over all processors. Message passing is required at the boundary nodes to adjacent processors to compute flux terms. PETSc provides highly efficient parallel solvers and preconditioners. Use of the distributed array (DA) parallel data structure provides a seamless construction of parallel vectors and communication between processors. Three different types of vectors can be distinguished: natural vectors associated with the physical coordinate system; local

vectors associated with each processor domain; and ghosted vectors which include boundary nodes from neighboring processors. Input properties, such as porosity and permeability, are input in physical or natural coordinates and then transformed to coordinates local to each processor. The DA implementation, however, is restricted to structured grids, although PETSc also provides data structures for unstructured grids. A general check of the parallel implementation is to note that the number of time steps, Newton iterations, and time step cuts should be independent of the number of processors, with some exception allowed for large numbers of processors due to degradation in preconditioning.

In PFLOW and PTRAN different approaches are used to implement the PETSc parallel routines. PFLOW is based on the nonlinear solver in PETSc referred to as SNES. In the SNES algorithm a system of nonlinear equations are solved directly and the user need only provide the residual function and Jacobian matrix. PTRAN, by contrast, uses the PETSc routines to solve a linear problem at each Newton iteration using the linear solver routines referred to as KSP (formally named SLES).

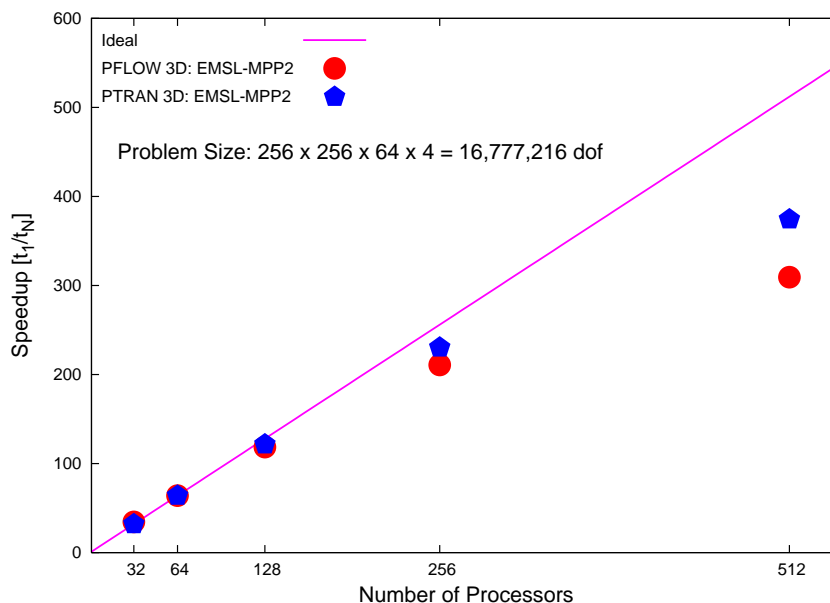


Figure 3: Speedup curves for PFLOW and PTRAN for an  $x$ - $z$  problem on a 3D grid  $256 \times 64 \times 256$  with 4 degrees of freedom per node.

Parallel speedup for PFLOW and PTRAN with up to 512 processors is shown in Figure 3 for a 3D problem involving injection of  $\text{CO}_2$ . For PTRAN a 4-component system was used with primary species:  $\text{Ca}^{2+}$ ,  $\text{H}^+$ ,  $\text{SiO}_2(\text{aq})$ , and  $\text{CO}_2$ . Calculations were carried out on Mpp2 (1960 Itanium-2, 1.5 GHz processors with Quadrics QsNetII interconnect) at the Molecular Sciences Computing Facility in EMSL located at PNNL. A grid with dimensions  $256 \times 64 \times 256$  with 1 m grid spacing and with 4 equations per node, giving a total of 16,777,216 degrees of freedom, was used. This corresponds to a single processor domain, for example, of  $16 \times 16 \times 32$ . As can be seen from the figure, speedup begins to decline above 256 processors. PTRAN gives slightly better results compared to PFLOW for more than approximately 256 processors. Still with 512 processors a speedup of 300–400 is obtained, which is quite reasonable considering the preliminary nature of the results. Better efficiency is expected as the code parallelization is improved. PETSc has a number of tools available for analyzing run time efficiency which have yet to be implemented.

## 4 Application to Geologic CO<sub>2</sub> Sequestration

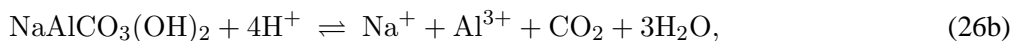
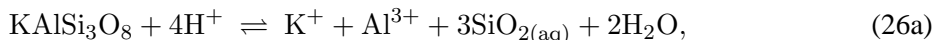
In this section an example is presented for CO<sub>2</sub> diffusion into a carbonated arkosic sandstone and the effects of convective mixing on mineral alteration. The composition of the sandstone is listed in Table 1. The effective rate constants (product of specific mineral surface area and kinetic rate constant) used in the simulation is also listed. These values are highly uncertain on depend on grain size, surface roughness and solution composition (Dove, 1999). A domain measuring 64 m × 128 m with a grid spacing of 1 m is considered. The system is initially in hydrostatic equilibrium with a pressure at the top of the domain of 20 MPa and temperature of 50°C with a geothermal gradient of 0.025°C/m. No flow boundary conditions are imposed at the sides and bottom of the domain, and a fluid in equilibrium with a fixed CO<sub>2</sub> concentration of 170 bars is imposed at the top. The initial fluid has pH 8 and is in equilibrium with respect to the primary minerals in the sandstone formation. The CO<sub>2</sub>-saturated fluid at the top boundary is also in equilibrium with respect to the sandstone primary minerals, but with a lower pH of 4.5.

Table 1: Carbonated sandstone composition and effective kinetic rate constants used in the model simulations.

Mineral	Volume Fraction	Effective Rate Constant
	—	mol/cm <sup>3</sup> /s
Quartz	0.55	1 × 10 <sup>-16</sup>
K-feldspar	0.20	1 × 10 <sup>-14</sup>
Calcite	0.10	1 × 10 <sup>-08</sup>
Dolomite	0.00	1 × 10 <sup>-10</sup>
Dawsonite	0.00	1 × 10 <sup>-12</sup>
Kaolinite	0.00	1 × 10 <sup>-12</sup>
porosity	0.15	

Shown in Figure 4 is the concentration of Ca<sup>2+</sup> in equilibrium with calcite for the system Ca<sup>2+</sup>-Na<sup>+</sup>-Cl<sup>-</sup>-CO<sub>2</sub>-H<sub>2</sub>O plotted as a function of pH at 50°C. Also shown is the corresponding CO<sub>2</sub> partial pressure. The Ca<sup>2+</sup> concentration increases with decreasing pH and increasing NaCl concentration, the latter caused by complexing with NaHCO<sub>3</sub><sup>-</sup>. As can be seen from the figure, at high CO<sub>2</sub> partial pressures equilibrium with respect to calcite can be achieved even for relatively low pH with reasonable Ca<sup>2+</sup> concentrations. This result suggests that a CO<sub>2</sub>-saturated brine will eventually dissolve a sufficient quantity of calcite to come to equilibrium and thus calcite should remain relatively stable following CO<sub>2</sub> injection, except near the injection well. It should be noted that this analysis does not take into account the change in solubility of CO<sub>2</sub> in the presence of NaCl (Duan and Sun, 2003).

For aluminosilicate minerals and formation of dawsonite the situation is somewhat different. In this case an equilibrium state does not exist at high CO<sub>2</sub> concentrations, and the mineral assemblage dawsonite-K-feldspar-quartz is incompatible. Consider the simultaneous reactions



for K-feldspar and dawsonite, respectively. Subtracting gives the overall reaction for dawsonite replacing K-feldspar



The mass action equation for this reaction reads

$$\frac{a_{\text{K}^+}}{a_{\text{Na}^+}} = \frac{K_{\text{kspar}} K_{\text{CO}_2} P_{\text{CO}_2}}{K_{\text{daw}} a_{\text{SiO}_2(\text{aq})}}, \quad (28)$$

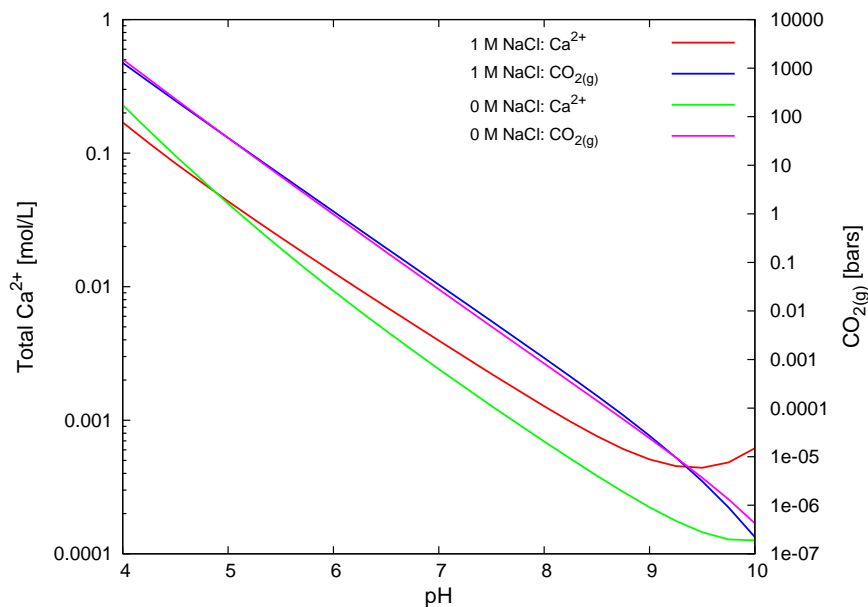


Figure 4: Solubility of calcite plotted as a function of pH with and without the presence of a NaCl brine. Also shown is the corresponding CO<sub>2</sub> partial pressure.

with  $P_{\text{CO}_2}$  the partial pressure of CO<sub>2</sub>. At 50°C,  $K_{\text{ksp}^{\text{par}}} = 10^{-0.73}$ ,  $K_{\text{daw}} = 10^{9.58}$ , and  $K_{\text{CO}_2} = 10^{-1.71}$ . To bracket possible silica concentrations note that the log  $K$  for quartz and chalcedony at 50°C are  $K_{\text{qtz}} = 10^{-3.59}$  and  $K_{\text{chal}} = 10^{-3.34}$ , respectively. Substituting these values gives for the potassium to sodium ratio values of 4.16 and 0.74 for equilibrium with quartz and chalcedony, respectively, at  $P_{\text{CO}_2} = 200$  bars. For Na<sup>+</sup> concentrations on the order of 2 m or larger, gives extremely large K<sup>+</sup> concentrations (~10 m) for equilibrium with quartz. This result implies that under high CO<sub>2</sub> concentrations, quartz and K-feldspar must dissolve as dawsonite precipitates and that the reaction will continue until the CO<sub>2</sub> concentration drops or one of the reactants is consumed.

As the system evolves in time, the high CO<sub>2</sub> concentration at the upper boundary diffuses downward into the domain increasing the density of the initial fluid present in the sandstone pores and thereby causing a density instability (Ennis-King and Paterson, 2003; Garcia, 2003). To seed the instability, white noise is added to the permeability which is assumed to have an average value of  $10^{-14}$  m<sup>2</sup>.

As can be seen in Figure 5(a) showing the mol fraction of dissolved CO<sub>2</sub> after an elapsed time of 200 years, fingering develops with lobes of high CO<sub>2</sub> concentration migrating downward. The corresponding pH profile is shown in Figure 5(b). The pH ranges from the initial pH value of 8 to approximately 4.8 at the center of the high CO<sub>2</sub> lobes. The concentrations for Ca<sup>2+</sup>, SiO<sub>2(aq)</sub>, K<sup>+</sup>, and Al<sup>3+</sup>, and are shown in Figures 6(a, b) and 7(a, b), respectively.

The resulting mineral alteration over the time span of 200 years is found to be minimal, even for carbonate minerals. Shown in Figure 8(a) is the volume fraction of kaolinite, and in Figure 8(b) the volume fraction of dawsonite. Dawsonite forms in the high CO<sub>2</sub> and low pH regions corresponding to the fingers, whereas kaolinite forms in the low CO<sub>2</sub> and high pH regions between the fingers. Note the interlocking relative positions of the two phases as shown in the figures. Given longer times (~10<sup>4</sup> years), significantly greater alteration is expected to occur for these minerals.

## 5 Conclusions

The PETSc library for parallel computing was successfully implemented in PFLOTRAN, providing speedups of up to 300-400 for 512 processors for a 3D problem with  $256 \times 64 \times 256$  nodes. A simple example problem was used to illustrate the application of the code to CO<sub>2</sub> sequestration in a carbonated sandstone. It was found that calcite was surprisingly stable, even under the low pH conditions produced by the high CO<sub>2</sub> concentrations. Kaolinite and dawsonite were found to precipitate in small quantities after an elapsed time of 200 years. However, over geologic times significant alteration could occur. To resolve fingering patterns resulting from density instabilities as CO<sub>2</sub> dissolves into the ambient aquifer fluid, relatively small grid spacing is required on the order of a meter. This will place stringent limitations on the grid resolution of field scale simulations to resolve such details. In this regard, parallel computing combined with adaptive mesh refinement techniques will be essential.

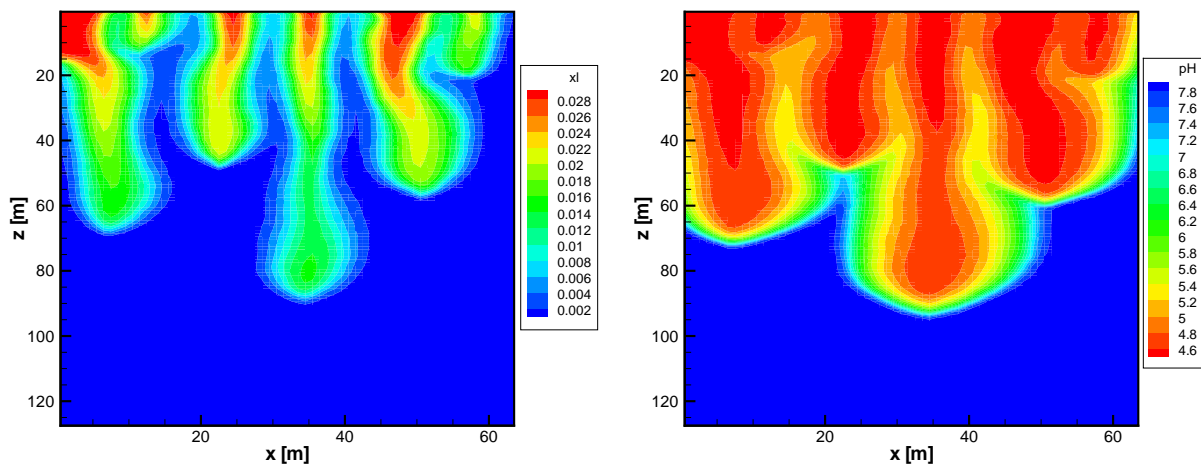
## Acknowledgments

This research was performed in part using the Molecular Science Computing Facility (MSCF) in the William R. Wiley Environmental Molecular Sciences Laboratory, a national scientific user facility sponsored by the U.S. Department of Energy's Office of Biological and Environmental Research and located at the Pacific Northwest National Laboratory. Pacific Northwest is operated for the Department of Energy by Battelle. The authors would like to thank Weonshik Han for providing a two-phase CO<sub>2</sub> injection problem using TOUGH2 to benchmark PFLOTRAN.

## 6 References

- Balay, S., W.D. Gropp, L.C. McInnes and B.F. Smith (1997) Efficient Management of Parallelism in Object Oriented Numerical Software Libraries, *Modern Software Tools in Scientific Computing*, Ed. E. Arge, A. M. Bruaset and H. P. Langtangen, 163–202, Birkhauser Press.
- Crovetto, R. (1991) Evaluation of solubility data of the system CO<sub>2</sub>-H<sub>2</sub>O from 273K to the critical point of water. *Journal of Physical and Chemical Reference Data*, 20(3), 575–589.
- Dodds, W.S., L.F. Stutzman, and B.J. Sollami (1956) Carbon dioxide solubility in water. *Industrial and Engineering Chemistry*, 1(1), 92–95.
- Dove, P.M. (1999) The dissolution kinetics of quartz in aqueous mixed cation solutions. *Geochimica et Cosmochimica Acta*, **63**, 3715–3727.
- Duan, Z., and R. Sun (2003) An improved model calculating CO<sub>2</sub> solubility in pure water and aqueous NaCl solutions from 273 to 533 K and from 0 to 2000 bar. *Chemical Geology*, 193, 257–271.
- Duan, Z., Moller, N., and Weare, J.H. (1992) An equation of state for the CH<sub>4</sub>-CO<sub>2</sub>-H<sub>2</sub>O system: I. Pure systems from 0 to 1000°C and 0 to 8000 bar. *Geochimica Cosmochimica Acta*, **56**, 2605-2617.
- Ennis-King, J., and P. Lincoln (2003) Role of convective mixing in the long-term storage of carbon dioxide in deep saline formations. In *SPE Annual Technical Conference and Exhibition*, Denver, CO, SPE 84344.
- Garcia, J. (2003) *Fluid dynamics of carbon dioxide disposal into saline aquifers*. Ph.D. Thesis, Berkeley, CA.
- Holt, T., J.-I. Jensen, and E. Lindeberg (1995) Underground storage of CO<sub>2</sub> in aquifers and oil reservoirs, *Energy Convers. Mgmt*, 36, 535–538.

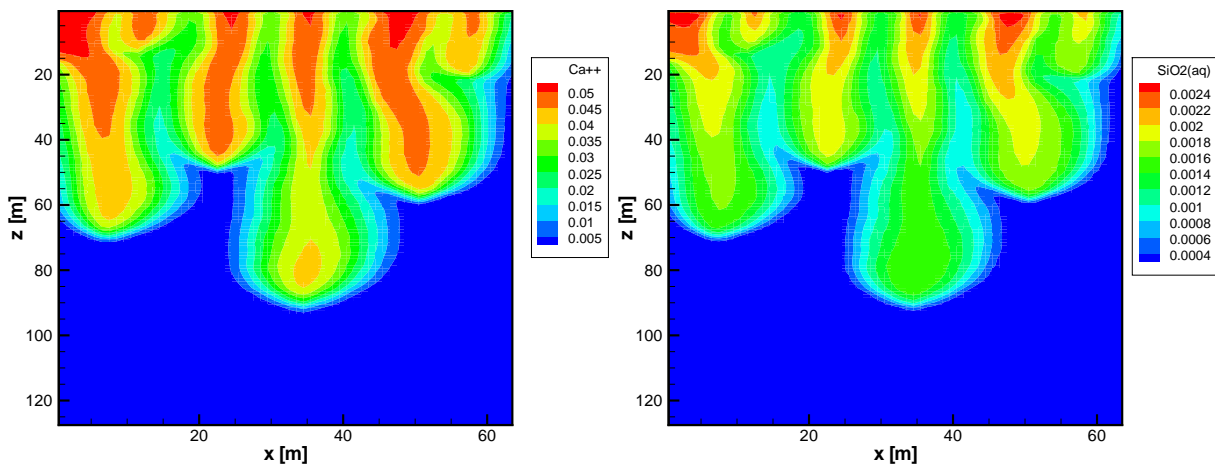
- Lichtner, P. C. and A. Wolfsberg (2004) Modeling Thermal-Hydrological-Chemical (THC) Coupled Processes with Applications to Underground Nuclear Tests at the Nevada Test Site; A Grand Challenge Supercomputing Problem. MPU Workshop: Conceptual Model Development for Subsurface Reactive Transport Modeling of Inorganic Contaminants, Radionuclides and Nutrients, Los Alamos National Laboratory, Report: LA-UR-04-1826.
- Lichtner, P. C., J. W. Carey, W. K. O'Connor, D. C. Dahlin, and G. D. Jr. Guthrie (2003) Geochemical mechanisms and models of olivine carbonation. Proceedings of the 28th International Technical Conference on Coal Utilization & Fuel Systems, March 9-13, 2003.
- Lindeberg E., and T. Holt (1994) EOR by miscible CO<sub>2</sub> injection in the North Sea, SPE 27767.
- Parker, J.C., R.J. Lenhard, and T. Kuppasamy (1987) A parametric model for constitutive properties governing multiphase flow in porous media, *Wat. Res. Res.*, **23**, 618–624.
- Pruess, K., C. Oldenburg, and G. Moridis (1999) TOUGH2 user's guide, version 2.0. Technical Report LBNL-43134, Lawrence Berkeley National Laboratory, Berkeley, CA.
- Span, R., and W. Wagner (1996) A new equation of state for carbon dioxide covering the fluid region from the triple-point temperature to 1100 K at pressures up to 800 MPa, *Journal of Physical Chemical Reference Data*, **25**, 1509–1596.
- Takenouchi, S., and G.C. Kennedy (1964) The binary system H<sub>2</sub>O-CO<sub>2</sub> at high temperatures and pressures. *American Journal of Science*, **262**, 1055–1074.
- Todheide, K., and E.U. Franck (1963) das zweiphasengebiet und die kritische kurve im system kohlendioxid-wasser bis zu drucken von 3500 bar. *Zeitschrift fur Physikalische Chemie Neue Folge*, **37**, 387–401.



(a) Mole fraction of dissolved CO<sub>2</sub>.

(b) pH

Figure 5: Plot of dissolved CO<sub>2</sub> mole fraction (left), and pH (right) after an elapsed time of 200 years.



(a) Ca<sup>2+</sup>

(b) SiO<sub>2(aq)</sub>

Figure 6: Plot of Ca<sup>2+</sup> (left), and SiO<sub>2(aq)</sub> (right) after an elapsed time of 200 years.

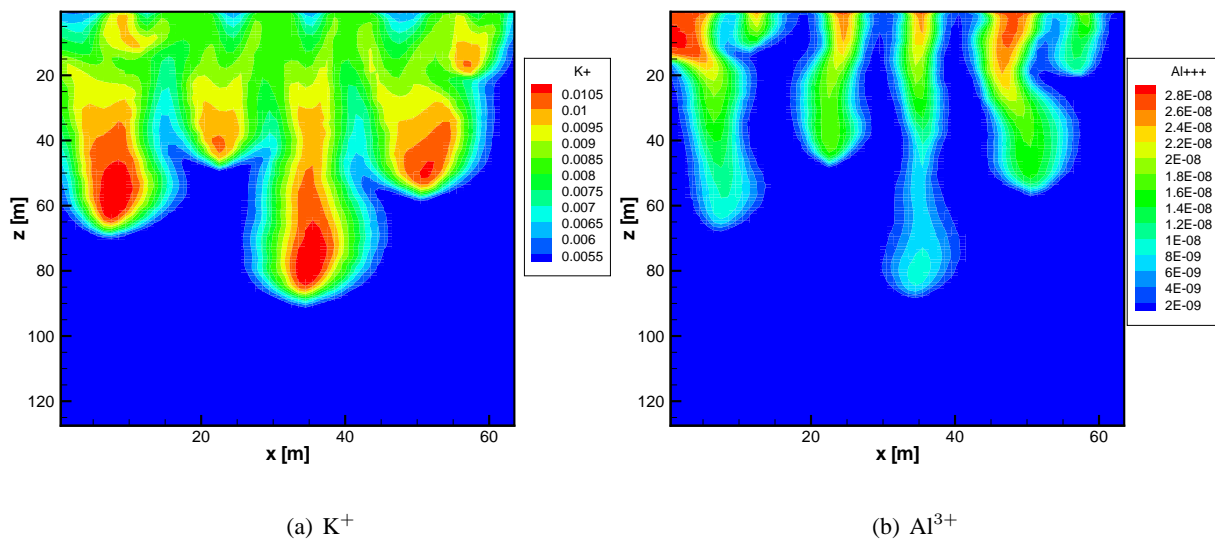


Figure 7: Plot of  $K^+$  (left), and  $Al^{3+}$  (right) after an elapsed time of 200 years.

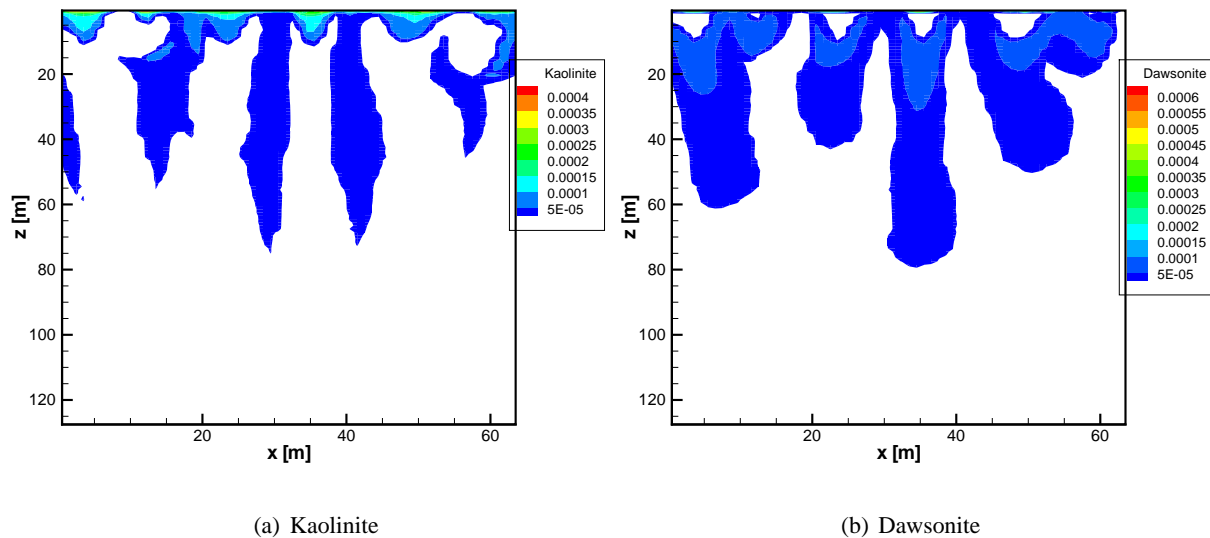


Figure 8: Plot of kaolinite (left), and dawsonite (right) volume fractions after an elapsed time of 200 years.